JOURNAL OF MECHANICAL ENGINEERING AND SCIENCES
ISSN: 2289-4659 e-ISSN: 2231-8380
VOLUME 19, ISSUE 4, 2025, 10863 - 10876
DOI: https://doi.org/10.15282/jmes.19.4.2025.3.0851

RESEARCH ARTICLE

Hybrid approaches for sheet metal formability prediction: A synergy of experimental, numerical and machine learning tools

Mounir Trabelsi[1], Boutheina B. Fraj[2], Hamdi Hentati[3,4]*, Taoufik Kamoun[1], Mounir B. Amar[5], Mohamed Haddar[4]

[1] Higher Institute of Technological Studies of Sfax, Route de Tunis km 10, B.P. 261, 3031 Sfax, Tunisia

[2] Nanomaterials and Systems for Renewable Energy Laboratory, Research and Technology Center of Energy, Technopole Borj Cedria, B.P. 95, 2050 Hammam Lif, Tunisia

[3] Higher School of Sciences and Technology of Hammam Sousse (ESSTHS), University of Sousse, Rue Lamine Abassi, 4011 Sousse, Tunisia

[4] LA2MP Laboratory, National School of Engineers of Sfax, University of Sfax, B.P. 1173, 3038 Sfax, Tunisia

[5] Laboratory of Process and Materials Sciences (LSPM), CNRS, Sorbonne Paris Nord University, 99 Avenue Jean Baptiste Clément, 93430 Villetaneuse, France

ABSTRACT - The optimization of sheet metal forming processes is a main goal in the mechanical industry, particularly in the widely used drawing technique. However, the lack of material databases concerning metal ductility presents significant challenges. To address this issue, this study develops machine learning (ML) methods to optimize the sheet metal forming process. The Erichsen cupping tests are employed to evaluate the formability and damage characteristics of A36 sheet parts, aiming for successful drawing outcomes. These tests consider three key parameters: punch diameter, friction between tools and sheet metal, and sheet thickness. Experimental findings show that punch diameter greatly affects the Erichsen index (*IE*). Microstructural analysis reveals a notable impact of sheet thickness on the maximum punch force (F_{max}), which is further confirmed by X-ray diffraction analysis. A finite element (FE) model based on the Johnson–Cook material law is developed to simulate the deep drawing tests. Numerical predictions show good agreement with experiments, with an average error of less than 4% for IE and 5% for F_{max}. By comparing numerical and experimental results, the isotropic model demonstrates satisfying and consistent performance. Using both experimental and numerical datasets, ML models are trained to predict *IE* and F_{max}. Among the tested algorithms (LR, RF, DT, SVR, and XGB), XGBoost (XGB) provides the most accurate predictions, with R^2 values of 99.60% for IE and 97.46% for F_{max}. The results indicate that XGB offers a robust and efficient approach for optimizing sheet metal forming processes through accurate prediction of formability and damage indicators.

ARTICLE HISTORY
Received : 06th Jun. 2025
Revised : 01st Nov. 2025
Accepted : 17th Nov. 2025
Published : 29th Dec. 2025

KEYWORDS
Forming tests
Sheet metal
Microstructural analysis
Plasticity and damage models
Machine learning

1. INTRODUCTION

Predicting mechanical and damage behavior to prevent strength degradation is a critical goal in materials science, engineering, and structural design [1, 2]. At the numerical level, several models have been developed to simulate damage in brittle and ductile materials. For brittle metals [3, 4], these models capture crack initiation and propagation, while for ductile materials, they focus on plastic deformation and fracture. Among them, the Johnson–Cook (J–C) constitutive and damage models are widely used to simulate manufacturing processes over a range of strain rates and temperatures [5, 6]. Their parameters are experimentally determined, providing strong agreement between finite element predictions and experimental outcomes [7, 8]. The J–C hardening model, in particular, has proven efficient in predicting forming behavior with high accuracy [9, 10] and is often applied under high strain rate and temperature conditions such as cutting and machining [10–12]. In the present work, attention is given to the drawing process, with an emphasis on the formability of sheet metals. The Erichsen cupping test is used to evaluate the punch penetration depth before fracture, offering key insights into forming ability as influenced by sheet thickness, punch diameter, and friction conditions [13, 14]. The accuracy of the formed part and surface quality depend strongly on avoiding cracking, wrinkling, and springback during drawing operations.

Several investigations have analyzed these influencing parameters. Studies involving normalized punch diameters have assessed the Erichsen index and deformation capability of metals [15], while others examined the effects of friction and clearance between tools and sheet metal on cup height and punch force [16, 17]. Experimental characterization of fracture cup height [18] and temperature effects in hot forming [19] have also been reported, demonstrating the role of thermal gradients in formability. The influence of friction and lubrication has been widely studied as well: Więckowski *et al.* [20] analyzed tribological aspects in titanium sheets, and Hia *et al.* [21] modeled stress–strain distributions showing that friction strongly impacts the plastic deformation behavior. Similarly, Szalai *et al.* [22] experimentally found that lubrication improves the Erichsen index of aluminum alloys by approximately 5 %, confirming the positive effect of friction control on formability. While these studies provide important understanding of mechanical and tribological effects, they remain mainly experimental or finite element (FE)-based. Few have addressed data-driven or hybrid

***CORRESPONDING AUTHOR | Hamdi Hentati** | ✉ hamdi.hentati@yahoo.fr

strategies to predict forming quality indicators such as the Erichsen index (*IE*) and maximum punch force (F_{max}). Recently, machine learning (ML) has emerged as a powerful tool for predicting and optimizing manufacturing outcomes, significantly reducing experimental costs and time [23–25]. Most reported works have applied ML, particularly Artificial Neural Networks (ANNs), to processes such as cutting and machining [26, 27]. However, systematic integration of finite element modeling (FEM) and ML for the Erichsen test, especially for A36 steel, has not yet been explored.

The present study bridges this gap by proposing a hybrid experimental–numerical–ML framework for A36 sheet metal. Experimental Erichsen tests are performed using various punch diameters to measure *IE* and F_{max}. A modified Johnson–Cook model is developed to describe the material behavior, and its parameters are calibrated using tensile tests. The FE simulations are validated against experimental data, followed by the training of ML algorithms, which are Linear Regression, Random Forest, Decision Tree, SVR, and XGBoost (XGB), to predict *IE* and F_{max}. Among these, XGB demonstrates the highest predictive accuracy, offering a robust and efficient approach for optimizing sheet metal forming processes.

2. MATERIALS AND METHODS

The Erichsen test is considered as deep drawing process. It serves the purpose of measuring the deep-drawing characteristics and ductility of sheet metal materials. During the test, a hemispherical punch is employed to transform a sheet metal sample into a cup-like shape. The measurement involves determining the depth at which the punch penetrates before the material cracks. The studied material, A36 structural steel, is a low carbon manganese steel. It is distinguished by its excellent resistance to impact. The modulus of elasticity (*E*) is 210 GPa, the yield strength (*YS*) is 220 MPa, and the ultimate tensile strength (UTS) is 340 MPa. Table 1 shows its chemical composition.

Table 1. Chemical compositions of the A36 sheet steel (wt%)

C	Mn	P	S	Si
0.25	1.03	0.04	0.05	0.28

In the current research, A36 sheet parts are subjected to drawing tests using a tensile machine. A load cell with a maximum capacity of 50 kN is employed, and a constant displacement rate of 5 mm/min is applied. To illustrate the material failure, the best criterion is the maximum load. In order to highlight this critical load, it is required to determine the load-displacement points for each time. Experimental tests were conducted with five punches that have different diameters (*d*), as illustrated in Figure 1. Two thicknesses, *s* =1 mm and *s* =2 mm, were used for the examined blanks.

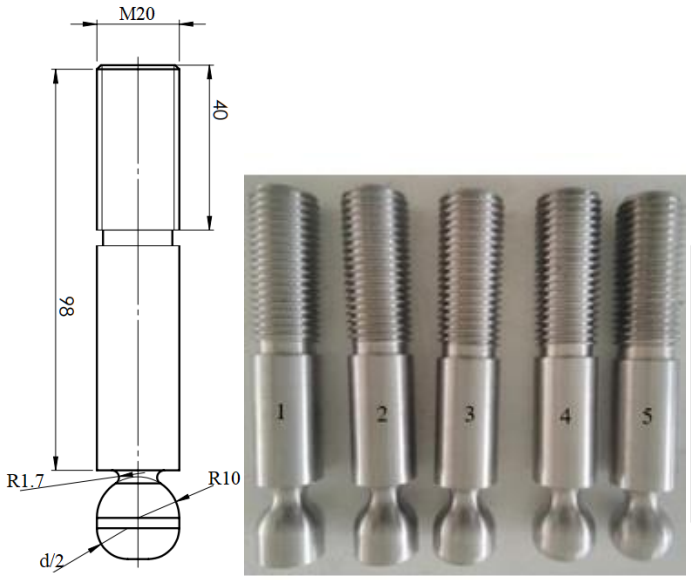

N° punch	d (mm)
1	0
2	5
3	10
4	15
5	20

Figure 1. Punches with their dimensions used in Erichsen tests

3. EXPERIMENTAL RESULTS

Based on the load-punch displacement curves, the maximum load corresponding to the onset of cracking (F_{max}) and the indentation depth at failure, referred to as the 'Erichsen index' (*IE*), are determined. We present in Figure 2 the punch force versus the punch displacement curve for the case where *s* = 1 mm, *d* = 10 mm, and without lubricant. Each Erichsen test was performed three times to ensure result reproducibility. The average values of the obtained *IE* and F_{max} are measured and summarized in Table 2.

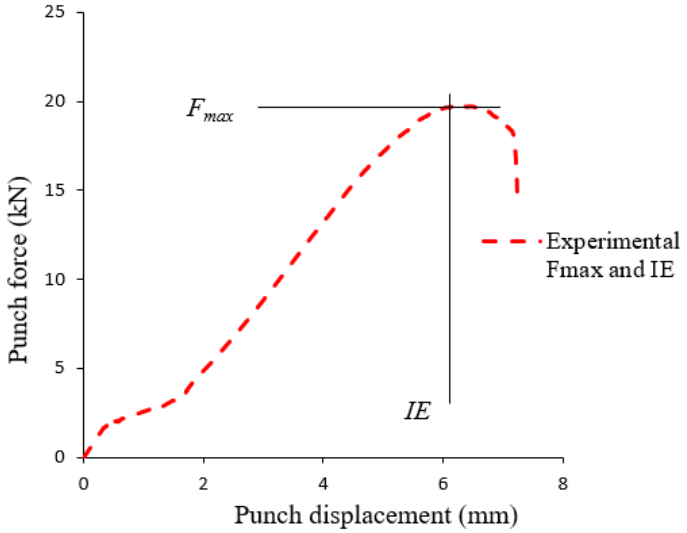

Figure 2. Experimental F_{max} and *IE*; in this case *s* = 1 mm and *d* = 10 mm and without lubricant

Table 2. Experimental results of Erichsen tests

Test	*s* (mm)	*d* (mm)	Average *IE* (mm)	Average F_{max} (kN)
1	1	0	3.1	14.4
2	2	0	3.5	31.4
3	1	5	5.1	19.0
4	2	5	5.7	39.3
5	1	10	6.5	19.8
6	2	10	7.4	38.6
7	1	15	8.1	19.0
8	2	15	9.1	39.8
9	1	20	9.5	17.7
10	2	20	10.8	36.7

Based on the data in Table 2, Figure 3 illustrates the effect of the two input parameters (*s* and *d*) on both *IE* and F_{max}. The punch diameter exerts a pronounced effect on the average *IE*. An increase from 0 mm to 20 mm results in a 206 % and 208 % rise for sheet thicknesses of 1 mm and 2 mm, respectively. Hence, the punch diameter's influence on the average *IE* appears to be largely independent of sheet thickness variation. On the other hand, we can observe, by means of the red dashed lines, that the influence of the sheet thickness on average *IE* depends on the punch diameter. When d increases, the impact of s becomes more significant. Referring to Table 2, for flat punch (*d* = 0 mm), by increasing *s* from 1 mm to 2 mm, average *IE* increases by 0.4 mm, whereas for *d* = 20 mm, this increase reaches 1.3 mm.

From Figure 3, it is worth noting that *d* has not remarkably altered the average F_{max}, regardless of the selected sheet thickness; except for *d* = 0 mm, when we note a moderate effect. However, significant increase of average F_{max} occurs when s varies from 1 mm to 2 mm. It can be concluded that an increase in sheet thickness results in an enhancement of F_{max}. The F_{max} value rises by more than 100 %. The notable impact of the sheet thickness on F_{max} appears to be intricately linked to a microstructural alteration within the examined material. To better elucidate this correlation, X-ray Diffraction (XRD) analysis was conducted to characterize possible phase transformations induced by the forming process. XRD analysis was conducted at room temperature, using a D8 Advance diffractometer with Cu Kα radiation (λ_{Cu} = 1.54A˚). Diffraction patterns were recorded over a 2θ range of 20°-100° for 30 minutes using a continuous scan, with a tube voltage of 40 kV and a tube current of 40 mA. The specimens were punched to a diameter of 20 mm, with thicknesses of 1 mm and 2 mm. As cast, the A36 microstructure is entirely in ferritic phase [28].

However, the XRD pattern of the punched 1 mm specimen (Figure 4(a)) reveals strong martensitic peaks, indicating that the high plastic strain and localized stress during drawing led to strain-induced martensitic transformation. This transformation is typical of low-carbon steels subjected to severe plastic deformation, where dislocation density increases and promotes the formation of α′-martensite from the original ferritic matrix. In contrast, the XRD pattern for the 2 mm specimen (Figure 4(b)) exhibits diffraction peaks corresponding to martensite, bainite, and cementite, revealing a mixed microstructure. The presence of bainite and cementite suggests that the thicker sheet experienced lower localized strain and heat generation, leading to partial transformation instead of full martensitic formation. This behavior indicates that

thickness-dependent deformation gradients influence the thermal and strain conditions during the punching process, thereby controlling the resulting microstructural phases.

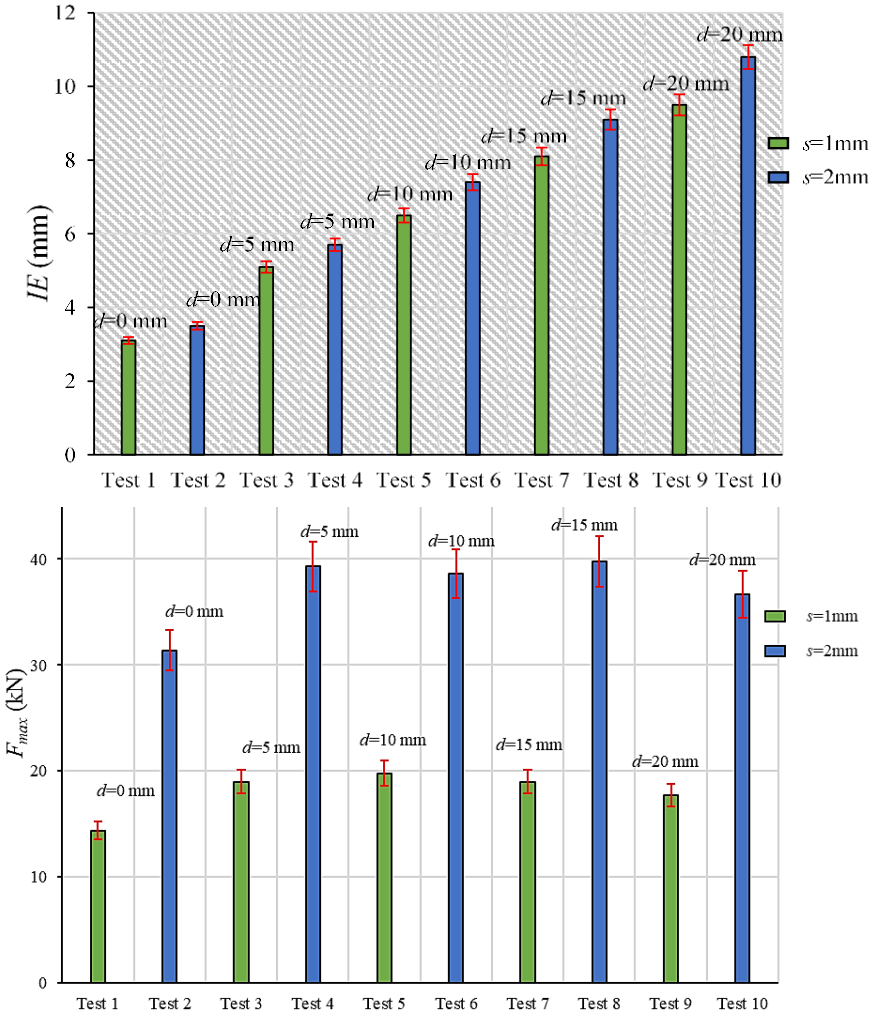

Figure 3. Average of measured *IE* and F_{max} for various tests

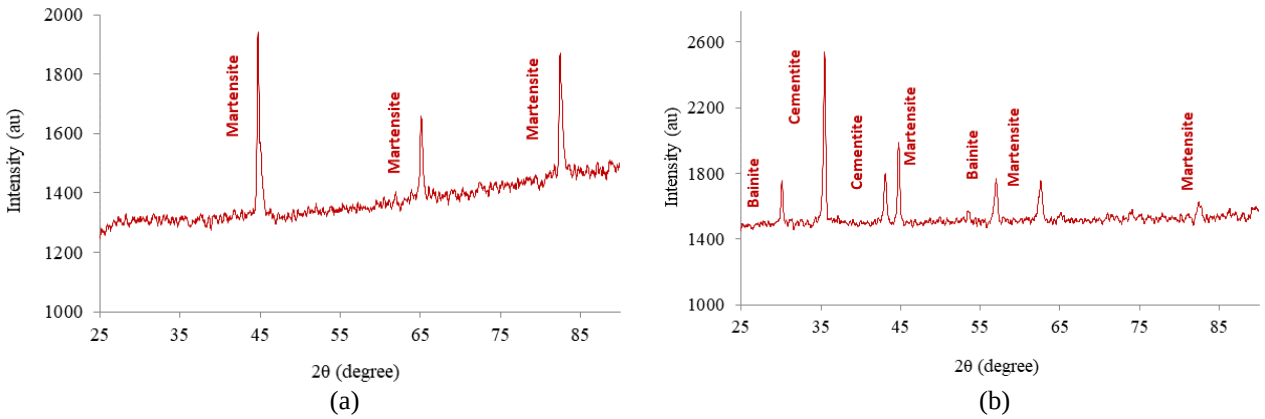

(a) (b)

Figure 4. XRD patterns of the punched sheet steel as a function of specimen thickness: (a) *s*=1 mm and (b) *s*=2 mm

These results confirm that the Erichsen forming process induces stress-assisted phase transformations, whose extent depends strongly on sheet thickness. The dominance of martensite in thinner sheets explains the higher F_{max} values observed experimentally, as martensitic microstructures exhibit higher strength and hardness but lower ductility. Conversely, the presence of bainite and cementite in thicker sheets contributes to slightly lower peak forces due to their relatively softer and more ductile nature. Based on the XRD data, the dislocation density (δ) within the punched A36 microstructure was calculated for both thicknesses, showing a notable increase for the 1 mm specimen. This further supports the conclusion that intense plastic deformation and strain localization promote defect accumulation and phase transformation, thereby affecting the forming response of A36 steel during the Erichsen test.

Figure 5 reports that increasing the sheet thickness, from s = 1 mm to s = 2 mm, leads to a decrease of the dislocation density, from 10.35 x 10^{-3} nm^{-2} to 6.4 x 10^{-3} nm^{-2}.

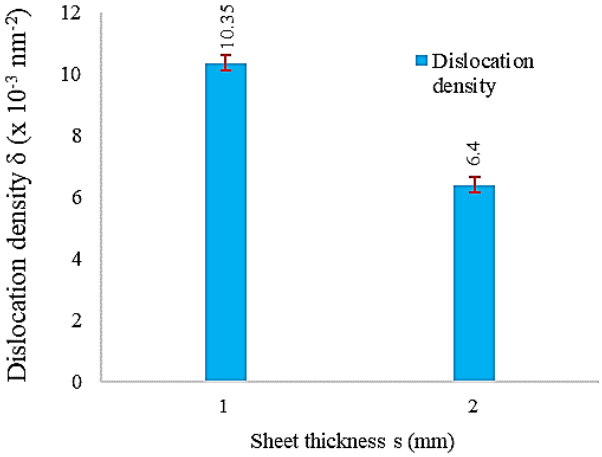

Figure 5. Dislocation density of the punched A36 sheet steel as function of specimen thickness

It is widely recognized that a reduction in dislocation density enhances material ductility by increasing resistance to both crack initiation and propagation. Consequently, it can be deduced that the intense increase of F_{max} as function of the sheet thickness could be attributed to the variation of this particular factor δ.

It is worth noting that while a classical ferrite-martensite transformation does not occur in A36 steel, extreme mechanical loading can create conditions where the material forms a new, ultra-hard phase that shares many characteristics with martensite or bainite [29]. This transformation is not predicted by equilibrium thermodynamics; it can be rationalized under extreme non-equilibrium conditions that fundamentally alter the material's energy state and phase stability. The most plausible scenario involves ultra-severe plastic deformation through high-pressure mechanical processes, where immense strain energy destabilizes the ferrite lattice and decomposes cementite, releasing carbon for trapping in a highly defective structure. This combination of mechanical destabilization and carbon redistribution can create a supersaturated, non-equilibrium phase exhibiting martensite-like hardness and microstructure. Alternatively, under extreme strain rates in adiabatic shear bands, localized deformation generates instantaneous heating above the austenitization temperature, followed by rapid self-quenching that may transform micro-scale volumes to martensite. Similarly, high-pressure shock loading can induce complex phase transformations through gigapascal pressures and rapid energy input. In all cases, the critical enablers are extreme mechanical forcing, whether through massive strain, high strain rates, or intense pressure, that provides the necessary energy to overcome thermodynamic barriers and create non-equilibrium phases with characteristics resembling martensite or bainite.

4. DAMAGE BEHAVIOR AND FRICTION MODELS

4.1 Plasticity model

With the purpose of developing a finite element model and predicting the damage mechanics of Erichsen tests, mechanical properties of the A36 sheet steel should be determined. Indeed, experimental tests are conducted in order to investigate the mechanical behavior. A set of experimental tensile tests are carried out on a tensile testing machine. Three orientations (0°, 45° and 90°) according to the rolling direction of sheet material were tested. Strain is measured using an extensometer, placed at half-length of the specimen. The stress-strain curves obtained from the tensile tests on sheet specimens are shown in Figure 6 with the different proposed orientations (0°, 45° and 90°).

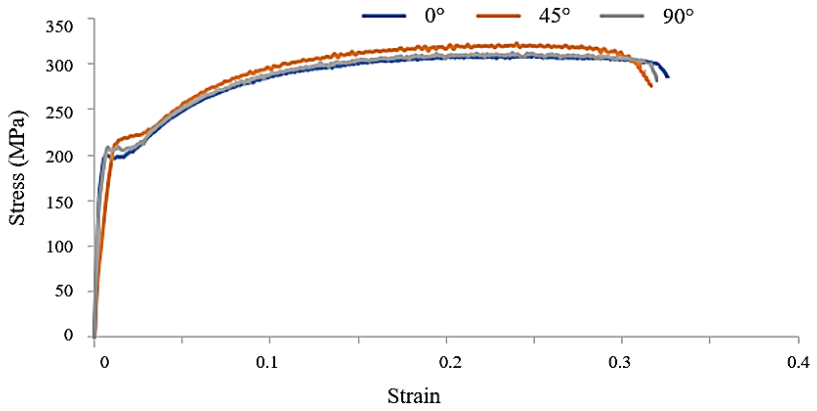

Figure 6. Conventional curves of sheet specimens

Figure 6 indicates that the Young's modulus remained unaffected by variations in sheet orientation. A slight variation in the values of elastic limit and tensile strength is observed. Therefore, A36 sheet steel with a thickness of 1 mm or 2 mm may be considered as an isotropic material. The used Johnson-Cook model neglects both strain rate and thermal softening effects. The flow stress σ_{eq} depends only on the equivalent plastic strain ε_{pl}. The plasticity law is given by Eq. (1).

$$\sigma_{eq} = \left(A + B\varepsilon_{pl}^{n}\right) \tag{1}$$

where *A, B and n* are material constants. The logarithmic form of Eq. (1) can be obtained by the Eq. (2):

$$ln\left(\sigma_{eq} - A\right) = n.Ln\left(\varepsilon_{pl}\right) + Ln(B) \tag{2}$$

The linear relationship plot between $ln(\sigma_{eq}- A)$ and $ln(\varepsilon_{pl})$ is drawn in Figure 7. A first-order regression model is fitted to the data points.

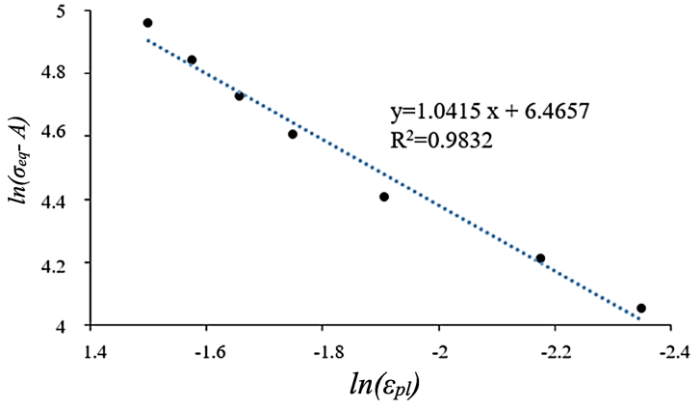

Figure 7. Logarithmic curve of Johnson-Cook hardening model

The logarithmic stress-strain curve, derived from tensile testing of specimens cut along three material orientations, is used to calibrate the modified Johnson-Cook hardening model (Eq. 1). The material constants are determined from the intercept of the fitted curve as follows: A = 245 MPa, B = 642.7 MPa, and n = 1.04.

4.2 Damage Model

The Johnson-Cook failure model (Eq. 3) expresses the fracture strain (ε_f) as a function of stress triaxiality (η), which is the ratio of the hydrostatic pressure to the equivalent stress. The effect of strain rate and temperature is neglected.

$$\varepsilon_f = (D_1 + D_2 e^{D_3 \eta}) \tag{3}$$

D_1, D_2 and D_3 are the damage model parameters.

Stress triaxiality quantifies the influence of the stress state on the material's failure strain. Damage modelling is based on the value of the cumulative damage parameter D_{JC} (Eq. 4). The material is undamaged when D_{JC} = 0 and is fractured at D_{JC} = 1.

$$D_{JC} = \sum \left(\frac{\Delta\varepsilon_{pl}}{\varepsilon_f}\right) \tag{4}$$

The material parameters must be determined through characterization tests. The triaxiality (Eq. 5), represents a dimensionless ratio of hydrostatic stress to Von Mises equivalent stress. It is a significant factor to control damage process.

$$\eta = \frac{\sigma_m}{\sigma_{eq}} \tag{5}$$

The Von Mises equivalent stress σ_{eq} is calculated as follow (Eq. 6):

$$\sigma_{eq} = \sqrt{\frac{1}{2}[(\sigma_1 - \sigma_2)^2 + (\sigma_2 - \sigma_3)^2 + (\sigma_3 - \sigma_1)^2]} \tag{6}$$

where σ_1, σ_2 and σ_3 are principal tensor stresses with the assumption that $\sigma_1 \geq \sigma_2 \geq \sigma_3$. The hydrostatic stress σ_m is calculated as following (Eq. 7):

$$\sigma_m = \frac{\sigma_1 + \sigma_2 + \sigma_3}{3} \tag{7}$$

The estimated stress triaxialities from the numerical simulations were found to be considerably consistent with the analytical solutions. The theoretical formula of stress triaxiality states, according to the sheet-grooved specimens subjected to the tensile loading [30], is given in Eq. (8).

$$\eta = \frac{\sqrt{3}}{3}\left[1 + 2\,ln\left(1 + \frac{t}{4R}\right)\right] \tag{8}$$

R and *t* are the radius of the notch and the thickness of the flat at the groove, respectively. Numerical characterization tests were performed on both bulk and sheet specimens in order to enable the examination of how the stress state evolves throughout the testing process [31–33]. By using various geometries in numerical characterization tests, several stress states are determined, and the damage behavior of these specimens is identified. In this section, various tensile tests are simulated. The triaxiality at failure is evaluated. It is computed for four smooth and notched specimens (SNS). The numerically determined triaxiality values were subsequently compared with analytical solutions obtained from Eq. (8). Furthermore, the complete stress states within the critical element of each sheet specimen were simulated. We present in table 3 the theoretical and computed triaxiality values at failure in the critical elements of notched specimens.

Table 3. Comparison between theoretical and numerical triaxiality values

Specimen	SNS_1	SNS_2	SNS_3	SNS_4
t(mm)	1	1	1	1
R(mm)	1	2	3	4
Numerical triaxiality	0.805	0.718	0.669	0.645
Theoretical triaxiality	0.835	0.713	0.67	0.647
Strain at failure	0.3	0.4	0.46	0.49

By substituting the stress triaxiality values and corresponding fracture strains into Eq. 3, the $\varepsilon_f = f(\eta)$ relationship is established, as shown in Figure 8. The model parameters D_1, D_2 and D_3 are subsequently determined from the coefficients of the fitted curve. These parameters, quantified in Table 4, enable prediction of ductile fracture in sheet steel during metal forming applications.

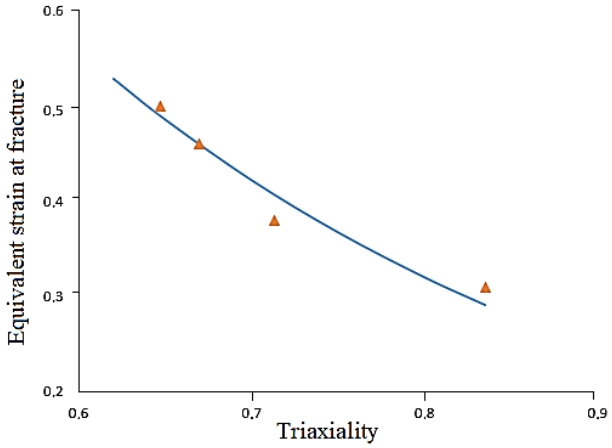

Figure 8. Relationship plot of equivalent strain at fracture ε_f and stress triaxiality η

Table 4. Failure constants of A36 sheet steel

D_1	D_2	D_3
0.03	3.2	-3

4.3 Friction Model

The accuracy of numerical simulations in metal forming processes is highly dependent on the friction model applied at the tool-workpiece interface. The selection of different friction models and coefficients significantly influences the predicted results, particularly the resulting stress states within the deformed material. The effectiveness of the combined Coulomb-Tresca friction model in metal forming simulations was proved in literature [10, 34]. In this regard, this friction model is described by the Eq. (9):

$$\tau_{fr} = \begin{cases} \mu_C.\sigma_n & if \quad \tau_{fr} < \tau_{\max} \\ m.\tau & if \quad \tau_{fr} \geq \tau_{\max} \end{cases} \tag{9}$$

where τ_{fr} is the shear friction stress, μ_C is the Coulomb friction coefficient, σ_n is the contact normal stress, m is the constant shear friction factor, τ is the shear flow stress and τ_{max} is the maximal shear stress. The combined Coulomb-Tresca friction model is thus applied in the current work, assuming that the Coulomb factor is $\mu_C = 0.25$ and the Tresca friction factor is $m = 0.45$.

5. COMPARISON BETWEEN NUMERICAL AND EXPERIMENTAL RESULTS

In the present section, the accuracy of the numerical model is checked by using the developed model for predicting the behavior of the material under Erichsen test. It is designed to form an indentation in a test piece by applying a

controlled force with different punch diameters. Finite element simulations of the Erichsen test were performed using Abaqus software. The blank holder, punch and die are considered as rigid bodies. The workpiece, however, is deformable. As boundary conditions, a constant displacement rate of 5 mm/min is imposed to the punch. The entire geometry of the workpiece is meshed using C3D8R elements, which are eight-node hexahedral element with selective reduced integration. With an imposed punch displacement, the reaction force for A36 sheet steel is numerically predicted and then compared with the experimental results. The simulations are carried out using the modified Johnson-Cook material models that are identified in the previous section. The Johnson-Cook plasticity model, in which, strain rate and temperature effects are not considered, allows us to predict deformation during the forming process. Furthermore, damage parameters were included in the Johnson-Cook failure model in order to study the fracture behavior. A mesh sensitivity analysis was conducted to ensure that the numerical results were independent of the mesh density. Several mesh configurations were tested by changing the element size from 0.2 mm to 0.8 mm in the punch–blank contact region. F_{max} and *IE* were used as reference quantities to evaluate convergence. The results showed less than 2 % variation in F_{max} and IE when the element size was reduced below 0.3 mm. Therefore, a mesh size of 0.3 mm was adopted for all subsequent simulations as a compromise between accuracy and computational efficiency. A summary of all material constants employed in the simulations is provided in Table 5.

Table 5. Material constants used in the simulations

m	μ_C	*A (MPa)*	*B (MPa)*	*n*	D_1	D_2	D_3
0.45	0.25	245	642.7	1.04	0.03	3.2	-3

A comparison between numerical prediction and the obtained experimental results should be made in order to validate the proposed Erichsen model. The load-displacement response is illustrated in Figure 9 for s=1 mm and d=10 mm. Good agreement is observed between experimental and numerical curves.

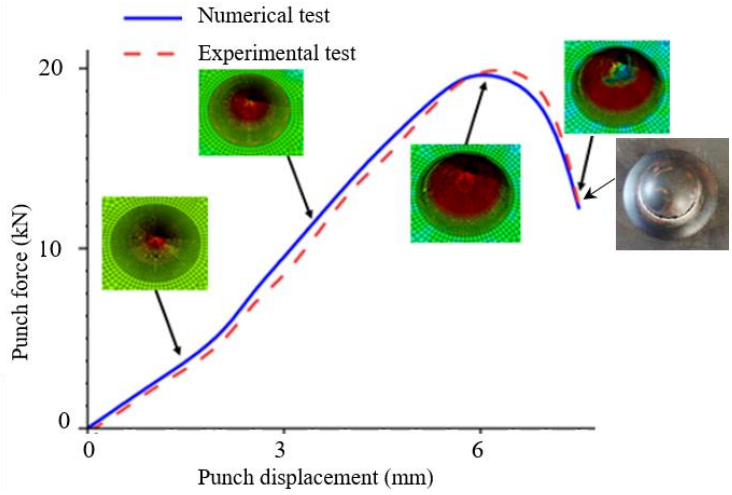

Figure 9. Load-displacement curves

Tables 6 and 7 show the main results related to Erichsen index (*IE*) and maximum force (F_{max}), respectively. Referring to Eq. (10), we determine the percent error of each result.

$$Error(\%) = \left| \frac{X_{num} - X_{\exp}}{X_{\exp}} \right| \times 100 \tag{10}$$

where X_{num} and X_{exp} represent the computed and the measured values, respectively.

Table 6. Comparison between experimental and numerical *IE*

Test	Sheet thickness (mm)	Punch diameter (mm)	*Experimental IE* (mm)	*Numerical IE* (mm)	*Error (%)*
1	1	0	3.1	3.28	5.8
2	2	0	3.5	3.81	8.86
3	1	5	5.1	5.21	2.16
4	2	5	5.7	5.68	0.35
5	1	10	6.5	6.55	0.77
6	2	10	7.4	7.48	1.08
7	1	15	8.1	8.36	3.21
8	2	15	9.1	9.32	2.42
9	1	20	9.5	9.75	2.63
10	2	20	10.8	11.1	3.74

Table 7. Comparison between experimental and numerical results of F_{max}

Test	Sheet thickness (mm)	Punch diameter (mm)	*Experimental* F_{max} (kN)	*Numerical* F_{max} (kN)	*Error (%)*
1	1	0	14.4	15.75	9.17
2	2	0	31.4	34.85	10.99
3	1	5	19	19.8	4.21
4	2	5	39.3	40.05	1.90
5	1	10	19.8	20.74	4.75
6	2	10	38.6	39.7	2.85
7	1	15	19	20.2	6.32
8	2	15	39.8	39.86	0.15
9	1	20	17.7	17.9	1.13
10	2	20	36.7	37.58	2.40

By comparing numerical to experimental results, we deduce that the use of isotropic model gives satisfactory results or good agreement. In fact, the modified Johnson–Cook (JC) models were employed. Unlike the classical JC formulation, the proposed version omits strain-rate and temperature dependencies, which are not significant under the quasi-static conditions of the Erichsen tests. This simplification facilitates parameter identification while maintaining high predictive accuracy. The incorporation of stress triaxiality (η) improves the description of ductile damage evolution. The resulting model shows better agreement with experimental data, as summarized in Tables 6 and 7, demonstrating its capability to accurately capture both plasticity behavior and fracture onset.

6. PREDICTION OF OUTCOMES USING MACHINE LEARNING MODELS

This section aims to predict F_{max} and *IE* through ML models using selected features including sheet thickness, punch diameter and friction between the sheet parts and tools. In fact, the lubrication is essential in metal forming operations, as it reduces friction and die wear, ultimately may enhance formability. To achieve this, both experimental and numerical tests were conducted under various friction conditions, including unlubricated and lubricated scenarios. In the experimental Erichsen tests, a commercial liquid lubricant based on mineral oil was applied to minimize friction between the punch, blank, and die surfaces. The lubricant was uniformly spread on both sides of the sheet and on the tool contact surfaces. The use of lubrication aimed to reproduce realistic forming conditions and to reduce frictional effects during deformation. In the numerical analysis, the Coulomb friction coefficient was set to $\mu_C = 0.25$ for unlubricated contact and $\mu_C = 0.1$ for the lubricated configuration, consistent with typical values reported for mineral oil lubricants in sheet metal forming. (Eq. 9). Results showed that while lubrication affects the Erichsen index, this effect is not significant (Figure 10).

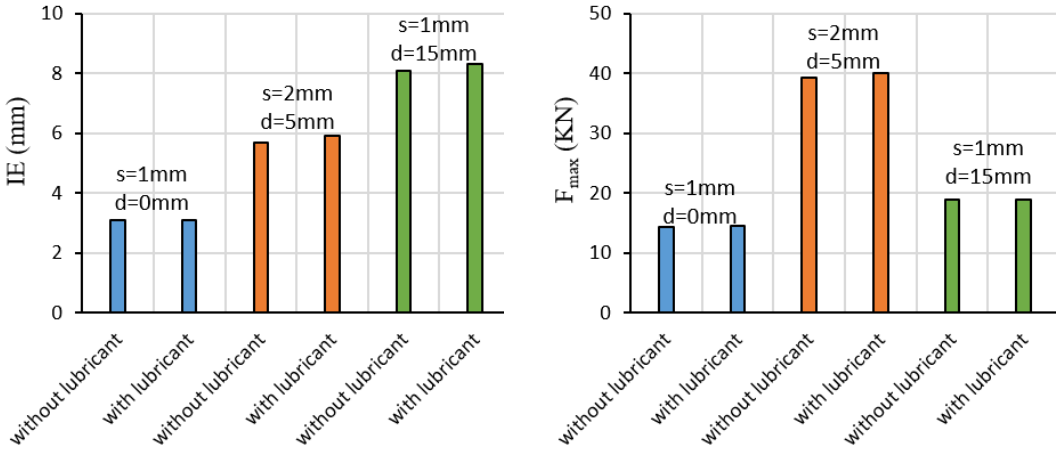

Figure 10. Lubrication effects on *IE and* F_{max}

Additionally, a series of experimental and numerical simulations explored the effects of sheet thickness, friction, and punch diameter, resulting in a dataset of 40 tests used to train ML models. These models effectively predict the *IE* and F_{max} required in forming operations, highlighting the critical role of these factors in optimizing metal forming processes. To demonstrate the influence of these Erichsen test parameters on predicting F_{max} and *IE*, a correlation matrix is used (Figure 11). The correlation coefficients represent the degree of linear association between pairs of variables.

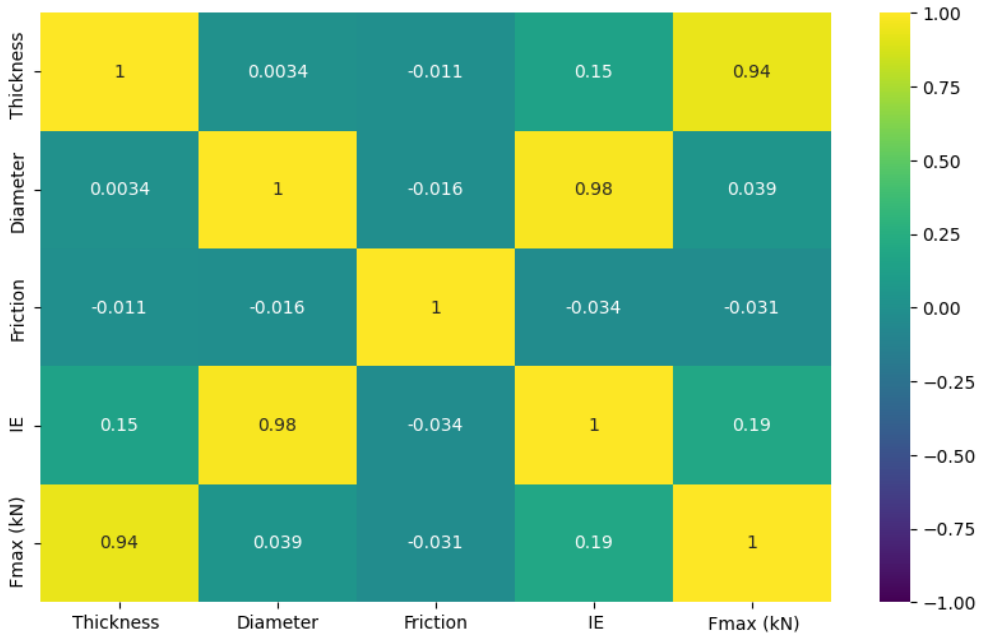

Figure 11. Correlation matrix representing the correlation coefficients between F_{max}, *IE* and Erichsen test parameters.

Analysis of this matrix reveals a strong linear relationship of 94 % between F_{max} and sheet thickness. Similarly, a high correlation of 98 % is observed between *IE* and punch diameter, underscoring a strong linear association. These results highlight the significant dependence of Erichsen outcomes on these process parameters. However, the correlation coefficient between friction and Erichsen test results is weak, indicating a slight negative relationship between friction and the Erichsen test results (F_{max} and *IE*). To predict F_{max} and *IE*, the following ML methods were employed: Linear Regression (LR), Random Forest (RF), Extreme Gradient Boosting (XGB), Decision Tree (DT) and Support Vector Regression (SVR). These techniques are widely recognized in ML modelling:

- LR establishes a linear relationship between independent and dependent variables by fitting a straight line to the data. LR models have been successfully used to accurately predict mechanical properties of industrial materials and composites.
- RF aggregates predictions from multiple decision trees, which helps to reduce overfitting and improve model generalization. RF regression demonstrates high accuracy in diverse engineering prediction tasks, particularly for modeling complex relationships in cutting processes. Its efficiency to handle small datasets makes it a preferred choice across studies [35, 36].
- XGB constructs an ensemble of weak learners sequentially, where each subsequent tree is optimized to correct the residual errors of the preceding ensemble. XGB regression is a greatly efficient method, which is widely applied in mechanical engineering prediction applications, particularly for nonlinear relationships with limited data [37, 38].
- DT splits the data into subsets based on the most informative features, forming a tree-like structure of decisions [39].
- SVR finds a hyperplane in a high-dimensional space that best fits the data within a defined margin [40].

The combined approach of experimental testing and numerical simulation, coupled with machine learning, provides a robust framework for understanding and optimizing the effects of sheet thickness, friction conditions, and punch diameter in axis-symmetric A36 sheet forming. In fact, for predictive modelling, the dataset comprises 40 combinations of thickness, punch diameter, and friction as input variables. The experimental determination of F_{max} and *IE*, serves as the target of this study and is used to train and evaluate our model. The data was divided into training and testing subsets, utilizing 70 % for training and 30 % for testing. It is noteworthy that the occurrence of outliers within this dataset is negligible. The accuracy of each model was evaluated using the R-squared (R^2) and the Root Mean Squared Error (RMSE) metrics, calculated according to Eq.s (11) and (12), respectively, as presented in Table 8 and plotted in Figure 12.

$$R^2 = 1 - \frac{\sum_{i=1}^{N}(y_i - \hat{y}_i)^2}{\sum_{i=1}^{N}(y_i - \bar{y}_i)^2} \tag{11}$$

$$RMSE = \sqrt{\frac{1}{N}\sum_{i=1}^{N}(y_i - \hat{y}_i)^2} \tag{12}$$

where y_i, $\hat{y}_i$ and $\bar{y}_i$ are, respectively, actual value, predicted value and mean of actual values. N is the number of data points.

Table 8. Metrics for the considered ML models

	F_{max} prediction		IE prediction	
	RMSE (%)	R^2 (%)	RMSE (%)	R^2 (%)
LR	11.05	88.47	3.59	98.66
RF	7.27	94.99	4.23	98.15
XGB	5.17	97.46	1.92	99.60
DT	6.69	95.76	2.30	99.44
SVR	10.54	89.53	4.48	97.85

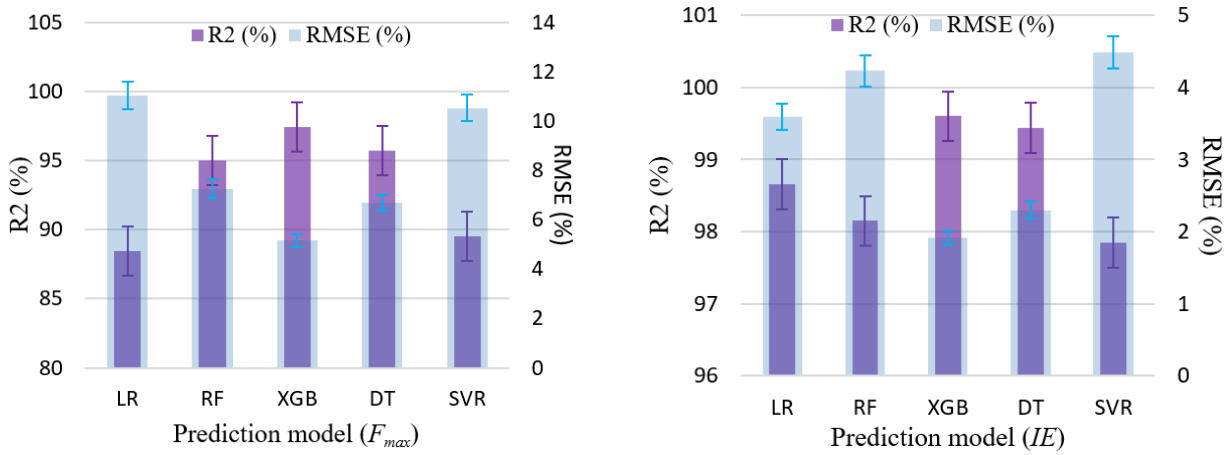

Figure 12. R^2 and RMSE of the selected ML models, for F_{max} (kN) and IE (mm)

As depicted in Figure 12, for the prediction of both F_{max} and IE, the XGB model demonstrates superior predictive performance compared to the other models. This is evidenced by its higher coefficient of determination (R^2), indicating a stronger linear relationship between the predicted and experimental values. Additionally, the XGB model exhibits the lowest root mean square error (RMSE), reflecting a smaller average deviation from the measured data and therefore improved prediction accuracy. These results suggest that the XGB algorithm effectively captures the nonlinear relationships and interactions between the input parameters, making it the most reliable model for predicting the mechanical responses of the tested steel sheets. Scatter plots of actual versus XGB predicted values of F_{max} and IE are presented in Figure 13.

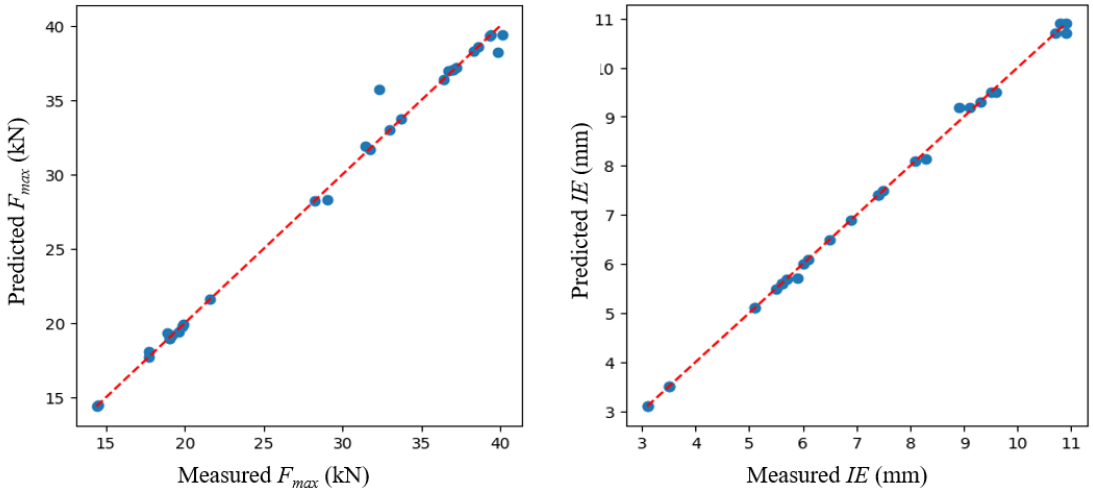

Figure 13. Scatter plots of actual vs XGB predicted values of F_{max} and IE

A scatter plot with high clustering around the diagonal line reflects that the XGB model is making very reliable predictions on this dataset. A correlation analysis was conducted to evaluate the influence of the input parameters on the mechanical responses F_{max} and IE. To quantify the relationship between the input parameters and the outputs (F_{max} and IE), the Pearson correlation coefficient was calculated as:

$$r = \frac{\sum_{i=1}^{N}(x_i - \underline{x})\left(y_i - \underline{y}\right)}{\sqrt{\sum_{i=1}^{N}(x_i - \underline{x})^2 \sum_{i=1}^{N}\left(y_i - \underline{y}\right)^2}} \quad (13)$$

where x_i and y_i are the values of the input and output variables, respectively, and $\underline{x}$ and $\underline{y}$ are their mean values.

The Pearson correlation coefficients show strong positive relationships: thickness (s) exhibits a correlation of approximately 0.97 with F_{max}, indicating that increasing the specimen thickness significantly enhances the maximum forming force and slightly increases the formability index. Similarly, punch diameter (d) shows strong correlations of 0.96 with F_{max}, confirming that larger punch diameters mainly improve the formability index while also slightly affecting the maximum force. These results demonstrate that both thickness and punch diameter are key parameters controlling the mechanical behavior of the specimens, providing a simple interpretability measure analogous to feature importance in machine learning models.

It is important to mention that the findings of this study should be interpreted considering the sample size (n = 40), which may limit the statistical power and broad generalizability of the results. While the dataset was sufficient to identify statistically significant trends and correlations, a larger sample would be required to confirm these relationships across all potential subpopulations and to detect smaller effect sizes with high confidence. However, several factors mitigate this limitation: i) the sample was carefully characterized and controlled for key variables, ensuring internal validity; and ii) the consistency of our results with established theories strengthens their plausibility. Therefore, while the results are robust within the defined experimental context, they should be validated in future studies with larger independent datasets.

7. CONCLUSIONS

The experimental results from tensile and Erichsen tests on A36 sheet parts provided a reliable database for validating the proposed numerical forming approach. Punch diameter was found to strongly influence the Erichsen index (IE), while sheet thickness significantly affected the maximum punch force (F_{max}). XRD analysis highlighted the effect of sheet thickness on the microstructural behavior of punched A36 steel. By combining 40 experimental tests with numerical simulations using a modified Johnson-Cook model, XGBoost-based machine learning models were developed to accurately predict *IE* and F_{max}, demonstrating the effectiveness of the hybrid experimental-numerical framework. This approach offers a valuable tool for optimizing forming processes. Future work will focus on expanding the dataset with additional numerical and experimental cases and exploring alternative machine learning algorithms to further improve predictive accuracy and generalization.

ACKNOWLEDGEMENTS

The authors would like to express their gratitude to the Machining Precision Company for the fabrication of the different tools to realize the different drawing tests.

FUNDING

This study was not supported by any grants from funding bodies in the public, private, or not-for-profit sectors.

CONFLICT OF INTEREST

The authors declare no conflicts of interest.

AUTHORS' CONTRIBUTION

M. Trabelsi (Conceptualization)

B. Ben Fraj (Conceptualization; Formal analysis)

H. Hentati (Writing - original draft)

T. Kamoun (Validation)

M. Ben Amar (Writing - review & editing)

M. Haddar (Writing - review & editing)

AVAILABILITY OF DATA AND MATERIALS

The datasets generated and/or analysed during the current study are available from the corresponding author on reasonable request.

ETHICS STATEMENT

This study did not involve human participants or animals. Ethical approval was therefore not required.

REFERENCES

[1] S. Moakhar, H. Hentati, M. Barkallah, J. Louati, M. Haddar, C. Bonk, "Modeling of ductile damage: Application for bar shearing," *Materialwissenschaft und Werkstofftechnik*, vol. 50, pp. 1353–1363, 2019.

[2] P. R. Ferreira Rocha, G. F. Gonçalves, G. dos Reis, R. M. Guedes, "Mechanisms of component degradation and multi-scale strategies for predicting composite durability: Present and future perspectives," *Journal of Composites Science*, vol. 8, no. 6, p. 204, 2024.

[3] O. Kayode, E. T. Akinlabi, "Investigation of microstructural and mechanical properties of AA1050–AZ91D dissimilar friction stir welding," *Journal of Mechanical Engineering and Sciences*, vol. 15, no. 3, pp. 8332–8343, 2021.

[4] H. Hentati, Y. Kriaa, G. Haugou, M. Haddar, "Influence of elastic waves on crack nucleation: Experimental and computational investigation of brittle fracture," *Applied Acoustics*, vol. 128, pp. 45–54, 2017.

[5] G. R. Johnson, W. H. Cook, "A constitutive model and data for metals subjected to large strains, high strain rates and high temperatures," in *Proceedings: 7th International Symposium on Ballistics*, The Hague, The Netherlands, 1983, pp. 541–547.

[6] G. R. Johnson, W. H. Cook, "Fracture characteristics of three metals subjected to various strains, strain rates, temperatures and pressures," *Engineering Fracture Mechanics*, vol. 21, no. 1, pp. 31–48, 1985.

[7] G. Li, S. Suril, T. Özel, "Material ductile failure-based finite element simulations of chip serration in orthogonal cutting of Ti-6Al-4V," *Journal of Manufacturing Science and Engineering*, vol. 141, no. 4, p. 041017, 2019.

[8] L. Y. Kou, W. Y. Zhao, X. Y. Tuo, G. Wang, C. R. Sun, "Effect of stress triaxiality on fracture failure of 6061 aluminium alloy," *Journal of Mechanical Engineering and Sciences*, vol. 14, no. 2, pp. 6961–6970, 2020.

[9] L. Ben Said, H. Hentati, T. Kamoun, M. Trabelsi, "Experimental and numerical investigation of folding process: Prediction of folding force and springback," *Mathematics*, vol. 11, p. 4103, 2023.

[10] L. Ben Said, M. Wali, "Accuracy of variational formulation to model thermomechanical problems and predict failure in metallic materials," *Mathematics*, vol. 10, no. 19, P. 3555, 2022.

[11] H. Hentati, I. B. Naceur, W. Bouzid, A. Maalej, "Numerical analysis of damage thermo-mechanical models," *Advances in Applied Mathematics and Mechanics*, vol. 7, no. 5, pp. 625–643, 2015.

[12] P. Löschner, M. K. Gupta, P. Niesłony, M. E. Korkmaz, M. Jamil, "Determination and verification of the Johnson–Cook constitutive model parameters in the precision machining of Ti6Al4V alloy," *Machines*, vol. 12, no. 10, p. 709, 2024.

[13] F. S. Sorce, S. Ngo, C. Lowe, A. C. Taylor, "Quantification of coating surface strains in Erichsen cupping tests," *Journal of Materials Science*, vol. 54, pp. 7997–8009, 2019.

[14] B. Ben Fraj, T. Kamoun, H. Hentati, M. Trabelsi, N. Ghazouani, M. Ahmed, "Optimization of forming force and Erichsen index using Taguchi design of experiments," *Proceedings of the Institution of Mechanical Engineers B*, vol. 238, no. 9, pp. 1316–1326, 2024.

[15] R. O. Santos, A. B. Pereira, M. C. Butuc, G. Vincze, A. J. Festas, L. P. Moreira, "Development of a device compatible with a universal testing machine to perform hole expansion and Erichsen cupping tests," *Machines*, vol. 8, no. 1, p. 2, 2020.

[16] D. Farioli, M. Fabrizio, E. Kaya, M. Strano, V. Mussi, "Reshaping of thin steel parts by cold and warm flattening," *International Journal of Material Forming*, vol. 16, p. 35, 2023.

[17] K. A. Francy and C. S. Rao, "Experimental investigation on the effect of process variables on quality characteristics of AA2024 processed by cold extrusion," *Journal of Mechanical Engineering and Sciences*, vol. 17, no. 3, pp. 9616–9628, 2023.

[18] M. Aydin, X. Wu, K. Cetinkaya, M. Yasar, I. Kadi, "Application of digital image correlation technique to Erichsen cupping tests," *Engineering Science and Technology, an International Journal*, vol. 21, no. 4, pp. 760–768, 2018.

[19] M. T. Nasri, F. Abbassi, F. Ahmad, W. Makhloufi, M. Ayadi, H. Mehboob, et al., "Experimental and numerical investigation of sheet metal failure based on Johnson–Cook model and Erichsen test," *Mechanics of Advanced Materials and Structures*, vol. 30, no. 7, pp. 2087–2100, 2022.

[20] W. Więckowski, J. Adamus, M. Dyner, M. Motyka, "Tribological aspects of sheet titanium forming," *Materials*, vol. 16, no. 6, p. 2224, 2023.

[21] J. Xia, J. Zhao, S. Dou, X. Shen, "A novel method for friction coefficient calculation in axis-symmetric deep drawing," *Symmetry*, vol. 14, no. 2, p. 414, 2022.

[22] S. Szalai, H. Csótár, D. Kurhan, A. Németh, M. Sysyn, S. Fischer, "Testing of lubricants for DIC-based forming limit diagram measurements," *Infrastructures*, vol. 8, p. 32, 2023.

[23] Q. Chen, Q. Xie, Q. Yuan, H. Huang, Y. Li, "Real-time monitoring of tool wear based on a convolutional Bi-LSTM model," *Symmetry*, vol. 11, no. 10, p. 1233, 2019

[24] R. Bobbili and V. Madhu, "Machine learning-based failure prediction of perforated plates under impact," *Mechanics Based Design of Structures and Machines*, vol. 50, no. 7, pp. 2582–2590, 2020.

[25] B. Ben Fathallah, R. Saidi, S. Belhadi, M. A. Yallese, and T. Mabrouki, "Modelling of cutting forces and surface roughness during straight turning of Stellite-6," *Journal of Mechanical Engineering and Sciences*, vol. 15, pp. 8540–8554, 2021.

[26] A. du Preez and G. A. Oosthuizen, "Machine learning in cutting processes as an enabler for smart sustainable manufacturing," *Procedia Manufacturing*, vol. 33, pp. 810–817, 2019.

[27] D. Umbrello, G. Ambrogio, L. Filice, R. Shivpuri, "A hybrid finite element method–artificial neural network approach for predicting residual stresses in hard turning," *Materials & Design*, vol. 29, no. 4, pp. 873–883, 2008.

[28] P. Zhang, Y. Chen, W. Xiao, D. Ping, X. Zhao, "Twin structure of lath martensite in low-carbon steel," *Progress in Natural Science: Materials International*, vol. 26, no. 2, pp. 169–172, 2016.

[29] M. Slewa, "Crystalline phase change due to high-speed impact on steel," *Journal of Material Sciences & Manufacturing Research*, vol. 6, no. 5, pp. 1–26, 2025.

[30] Y. Bai, X. Teng, and T. Wierzbicki, "Application of stress triaxiality in plane strain fracture testing," *J. Eng. Mater. Technol.*, vol. 131, no. 2, p. 021002, 2009.

[31] C. Hammami, N. Kammoun, H. Hentati, M. B. Amar, M. Haddar, "Parametric analysis of damage characterization tests of aluminium bulk material," *Journal of Mechanical Science and Technology*, vol. 36, pp. 5019–5025, 2022.

[32] M. Brünig, M. Zistl, S. Gerke, "Numerical analysis of damage and fracture behavior of preloaded aluminium alloy specimens," *Metals*, vol. 11, no. 3, p. 381, 2021.

[33] Y. Bao, T. Wierzbicki, "On fracture locus in equivalent strain and stress triaxiality space," *International Journal of Mechanical Sciences*, vol. 46, no. 1, pp. 81–98, 2004.

[34] Y. Aiman, S. Syahrullail, and A. H. Kameil, "Tribology in metal forming and bio-lubricants: A review," *Jurnal Teknologi*, vol. 86, no. 1, pp. 95–114, 2023.

[35] S. Bhandari, A. Shukla, "Prediction of responses in CNC milling using random forest regression," *Facta Universitatis, Series: Mechanical Engineering*, vol. 21, no. 4, pp. 685–700, 2023.

[36] M. Kateb, S. Safarian, "Machine learning-driven predictive modeling of mechanical properties in diverse steels," *Machine Learning with Applications*, vol. 20, p. 100634, 2025.

[37] S. Chakraborty, S. Bhattacharya, "Application of XGBoost as a predictive tool in CNC turning," *Reports in Mechanical Engineering*, vol. 2, no. 1, pp. 190–201, 2021.

[38] L. Ben Said, T. Kamoun, J. Mars, S. Alharbi, W. Rajhi, M. Turki, M. Wali, "Data-driven deep drawing optimization: Response surface methodology and machine learning," *Journal of Engineering Research*, in press, corrected proof, 2025.

[39] H. Dabiri, V. Farhangi, M. J. Moradi, M. Zadehmohamad, M. Karakouzian, "Tree-based machine learning for analysing ultimate strain of reinforcement bars," *Applied Sciences*, vol. 12, no. 10, p. 4851, 2022.

[40] Z. Che, C. Peng, "Improved support vector regression for predicting mechanical properties of low-alloy steel," *Mathematics*, vol. 12, no. 8, p. 1153, 2024.